Wavelet Based Denoising of Fractionated Intracardiac Electrograms

Niklas Tanger[1], Dylan Vermoortele[1], Hans Dierckx[2], Peter Haemers[1], Piet Claus[1]

[1] Department of Cardiovascular Sciences, KU Leuven, Leuven, Belgium
[2] Department of Mathematics, KU Leuven, Kortrijk, Belgium

Abstract

Fractionated intracardiac electrogram (EGM) recordings contain information about the underlying pathophysiology and are promising to guide clinical ablation procedures. Lowpass filters (LPF) are commonly used to denoise EGM recordings. An alternative is wavelet denoising which does not rely on a constant separation of signal and noise in frequency space. Unipolar and bipolar EGM recordings of 2.5 s registered during a contact mapping guided ablation procedure were exported from the Carto3® (Biosense Webster) mapping system. Different wavelet denoising algorithms are evaluated. The success in reducing noise while retaining the physiologically relevant signal morphology of each algorithm is assessed. For this purpose recordings with a prominent signal are selected such that a signal dominated interval and an isoelectric interval with dominant noise can be identified. The standard deviation of the deviation from baseline in the isoelectric interval are calculated to quantify noise. The change due to denoising in peak counts of bipolar voltages and the negative derivative of unipolar voltages during signal dominated intervals is calculated to quantify the stability of physiologically relevant morphology. The `han5.5` *wavelet with* `BlockJS` *thresholding and decomposition level 8 is identified as a successful choice for a denoising algorithm.*

1. Introduction

Catheter ablation guided by electroanatomic (EA) mapping is an established therapy for cardiac arrythmias. For example, pulmonary vein isolation is employed to treat atrial fibrillation (AF). Pathological myocardium can result in complex fractionation of the intracardiac electrograms (EGMs). Conduction velocity (CV) slowing is one of numerous underlying mechanisms that have been identified [1].

The potential to terminate persistent AF by targeting areas with fractionated signals has been explored without clear success [2]. There is currently no consensus on how to quantify fractionation. Peak counts of bipolar voltages or of the negative temporal derivative of unipolar voltages are examples of quantification used in the literature [3, 4]. Clinical EA mapping systems make standard use of LPFs to remove high frequency noise from the EGMs. Yet, high frequency components have been observed to contain relevant information for substrate identification [5].

Wavelet denoising algorithms offer an alternative that does not depend on a constant frequency cut off. Instead the recording is decomposed into components derived from a given "mother-wavelet" with local support. Threshold selection rules are then used to remove contributions due to noise and reconstruct the denoised signal. The performance of wavelet denoising depends on the interplay between the nature of the signal on the one hand and the chosen algorithm parameters such as wavelet type, thresholding rule and decomposition level on the other hand [6].

The goal of this study is to compare the performance of different wavelet denoising algorithms in removing noise from fractionated EGMs while preserving the pathophysiologic information conveyed by the signal morphology summarised as peak counts. LPF serves as a benchmark.

2. Methods

2.1. Data Acquisition

The EA activation map of a left atrium as well as the recordings of the 2251 points used for its generation were anonymised and exported from the Carto3® (Biosense Webster) mapping system after a mitral isthmus ablation procedure. The activation map consists of a mesh with values of local activation time (LAT) at each vertex. For each point the location of the electrodes at LAT annotation time, 2.5 s recordings of the bipolar and unipolar EGMs as well as the classic 12-lead electrocardiograms and the voltages recorded at reference electrodes placed in the coronary sinus were included in the export.

The use of the dataset has been approved by the local Ethics Committee Research UZ / KU Leuven as part of the project S67494.

 ISSN: 2325-887X DOI: 10.22489/CinC.2024.157

2.2. Data Analysis

The dataset was imported into MATLAB using OpenEP [7, 8]. Since the exported bipolar voltages were already strongly filtered, the difference between the unipolar voltages was used as the raw bipolar recording during the analysis. In each recording beats were segmented by association with the closest reference annotation calculated from voltages recorded in the coronary sinus [9]. Beats at the beginning and end of the recordings were excluded. Since the average cycle length of the mapped rhythm was 455 ms this resulted in 4 considered beats per recording point.

Recording points with a signal dominated interval separate from a noise dominated isoelectric interval were identified. As illustrated in figure 1, this was done by selecting points where in each considered beat the maximum of the unipolar voltage was followed by its maximal downslope which in turn was followed by its minimum while the maximum and minimum were separated by no more than 50 ms. 418 points met these criteria.

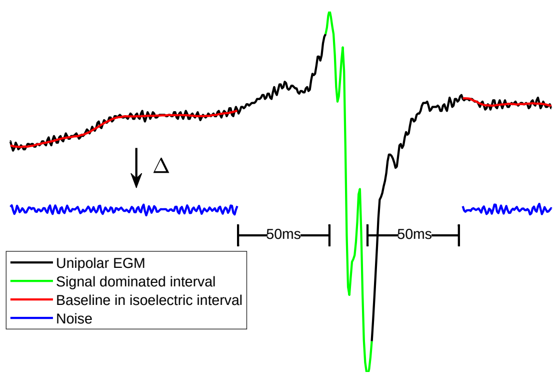

Figure 1: This figure illustrates the distinction between signal dominated interval and isolelectric interval in a beat of a unipolar EGM (black). The signal dominated interval (green) is between the peaks. In the isoelectric interval the noise (blue) is calculated as the difference between the EGM and the baseline (red).

The area between the extrema plus a 3 ms extension in both directions was defined as the signal dominated interval. The part of the recordings that was more than 50 ms away from both extrema was defined as isoelectric interval. For bipolar recordings both types of intervals were defined as the intersection of the respective intervals of both unipolar voltage recordings comprising the bipolar voltage.

In the isoelectric intervals, noise was defined as the difference of the voltage recording with a baseline determined by a Savitzky-Golay filter of order 5 with frame length of 11ms.

To assess the noise reduction of filtering algorithms, the noise was quantified in the raw voltage recordings as well as on the filtered voltage recordings. To obtain a single measure of noise for each algorithm, the empirical standard deviation of noise (σ_{Noise}) was calculated for each beat and the standard deviations were averaged over all ($n = 4 \times 418 = 1672$) beats.

To assess the signal preservation, peaks were counted in the signal dominated intervals. Peaks of bipolar (Bip) voltages and of the negative temporal derivatives of unipolar (Uni) voltages were counted in the raw voltage recordings as well as in the filtered voltage recordings. The absolute values of the differences ($\Delta N_{\mathrm{Peaks}}(\mathrm{Bip})$ and $\Delta N_{\mathrm{Peaks}}(-\frac{\mathrm{dUni}}{\mathrm{dt}})$) was averaged over all beats.

The analysis was performed for LPF as implemented in the "lowpass" function of MATLAB with the pass frequency varying from 50 Hz to 300 Hz in steps of 50 Hz. The analysed wavelet denoising algorithms were those that are implemented in MATLAB. Refer to the legend of figure 3 for a list of wavelet families and threshold selection rules.

2.3. Quantifying Fractionation

For 1856 voltage recordings within the left atrium (i.e. Points in one of the veins or the mitral valve were manually excluded based on their coordinates), fractionation was quantified in all 4 beats. This was done by counting either bipolar voltage peaks or peaks of the negative derivative of the unipolar voltage during the window of atrial activity, i.e. from 50 ms before until 200 ms after the reference annotation [9] of the respective beat.

For fractionation calculations peaks were identified as zero crossings of the derivative when the derivative exceeded a slope threshold. For each beat, the slope threshold was taken from the raw recordings as the maximum absolute value of the derivative outside of atrial activity.

The empirical standard deviation of the fractionation values over 4 consecutive beats of a given point ($\sigma^{\mathrm{B2B}}_{\mathrm{Frac}}$) was calculated to assess beat to beat variability.

3. Results

3.1. Difference between wavelet denoising and LPF

When varying the pass frequency of the LPF, the change in number of peaks in the signal dominated interval increases with increasing noise reduction. Thus, the choice of frequency forces a tradeoff between maintaining signal and reducing noise. In contrast to this, the change in number of peaks as well as the noise reduction converge when increasing the decomposition level of a wavelet denoising algorithm (see figure 2).

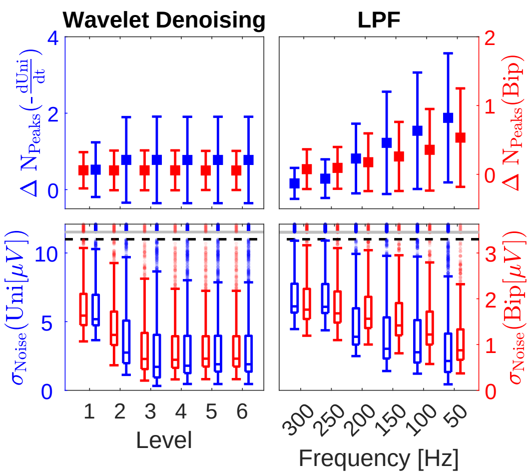

Figure 2: The upper figures show the change in peak number in the signal dominated intervals that was caused by the denoising algorithms (see section 2.2). Means and empirical standard deviation over all considered beats are shown. The lower figures visualises the distribution of the standard deviations of the remaining noise in the isoelectric intervals (see section 2.2) as boxplots. The black dashed and grey lines visualise that there are outliers outside the shown range. The Wavelet denoising algorithm in the left figures used `han5.5` wavelets and the `BlockJS` threshold selection rule.

3.2. Comparing wavelet denoising algorithms

Figure 3 compares the wavelet algorithms' ability to reduce noise while preserving peaks in the signal dominated intervals.

The best algorithms use the `BlockJS` threshold selection rule. For each combination of wavelet family and thresholding rule, only the wavelet with the biggest noise reduction and the wavelet with the smallest change in peak counts are shown. Of note, some of the wavelet denoising algorithms that are not included in the figure result in an increase in noise while distorting the number of peaks more than any of the analysed LPFs. An example of a wavelet denoising algorithm that is in this sense not suited for EGM denoising is using `rbio3.1` with `UniversalThreshold` selection rule.

Figure 4 shows a zoomed in part of figure 3 with some particularly successful wavelets emphasised.

3.3. Beat to Beat consistency of Fractionation

Figure 5 shows histograms of the beat to beat standard deviations of the fractionation calculated from bipolar voltages and the negative derivative of the unipolar voltages.

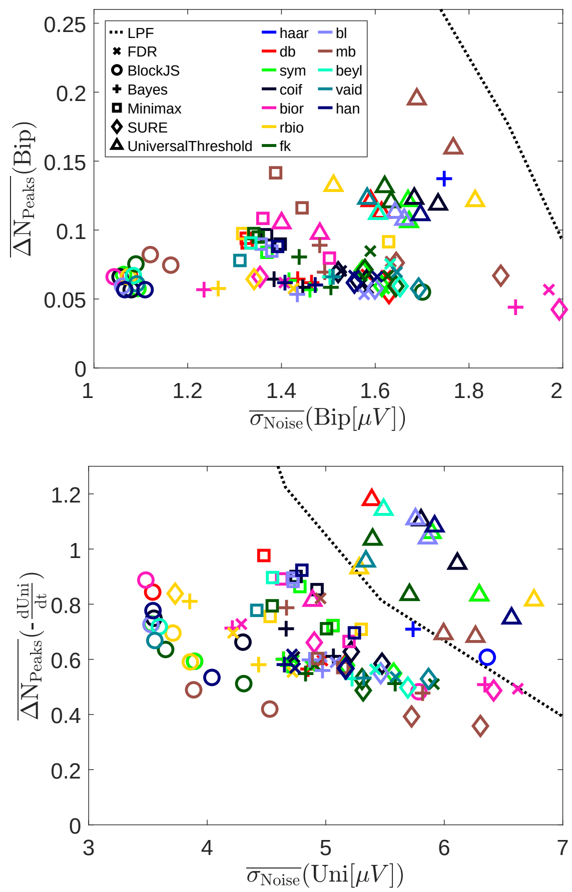

Figure 3: Mean peak change in signal dominated intervals are scattered against mean noise standard deviations in isoelectric intervals (see section 2.2). The level of all wavelet denoising algorithms was 8. Threshold selection rules are identified by markers while wavelet families are identified by colours. For each combination of threshold selection rule and wavelet family, the results for wavelets that resulted in the lowest mean peak change or the lowest remaining noise are shown. The dotted line results from connecting the results from the LPF algorithms with cut off frequency varied in steps of 50 Hz.

As expected denoising reduces the beat to beat variability because the electrophysiological signal is more consistent per beat than noise. Wavelet denoising with `BlockJS` thresholding and `han5.5` wavelets results in more bipolar recordings with minimal beat to beat fractionation variability than LPF with 200 Hz cut off frequency. Fractionation calculated from the derivative of unipolar voltages has similar consistency when calculated after this wavelet denoising or LPF.

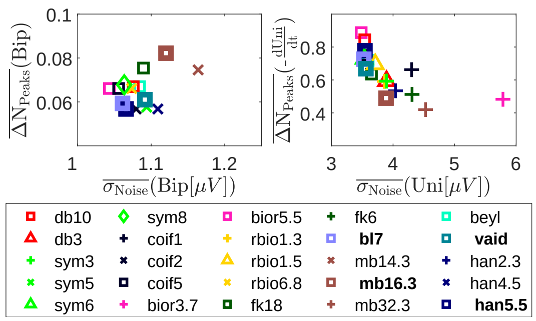

Figure 4: The same scatters as in figure 3 only here limited to `BlockJS` threshold selection are shown. Marker types identify the used wavelets. Some wavelets that are successful at reducing noise in bipolar and unipolar voltages while preserving the number for peaks in bipolar and temporal derivative of unipolar voltages are emphasised.

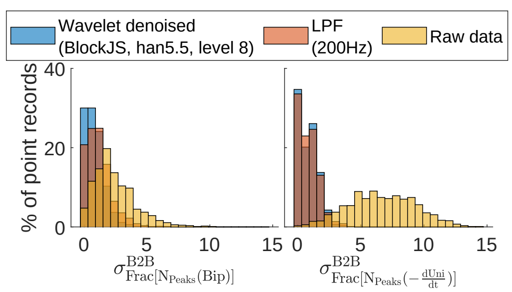

Figure 5: Histograms of the beat to beat variability of the fractionation calculated in 4 beats of each point (see section 2.3) are shown for fractionation calculated from raw, LPF and wavelet denoised bipolar and unipolar recordings.

4. Discussion

Wavelet denoising offers a way to distinguish noise from signal that does not depend on separation in the frequency domain. Compared to LPF wavelet denoising is not subject to the same trade off between noise reduction and signal preservation.

`BlockJS` threshold selection and the `han5.5` wavelet were identified as a denoising algorithm that works well for noise reduction and peak preservation for intracardiac EGMs. While this is not the only wavelet denoising algorithm that works, it is worth noting that poorer choices (e.g. `rbio3.1` wavelets with Universal Threshold selection rule) can fail terribly.

The increased beat to beat consistency of fractionation calculated from wavelet denoised recordings is consistent with the preserved morphology being physiological. However, this is not conclusive. For instance LPF with lower cut off frequencies also decrease the beat to beat variability of fractionation by consistently removing physiological high frequency contributions.

Acknowledgments

This project was supported by the KU Leuven internally funded project “Bayesian Inversion of Cardiac Electrograms for Patientspecific analysis (BICEPS)” IDN/22/006.

References

[1] de Bakker JM, Wittkampf FH. The pathophysiologic basis of fractionated and complex electrograms and the impact of recording techniques on their detection and interpretation. Circulation Arrhythmia and Electrophysiology April 2010; 3(2):204–213. ISSN 1941-3084.

[2] Waranugraha Y, Rizal A, Setiawan D, Aziz IJ. Additional complex fractionated atrial electrogram ablation does not improve the outcomes of non-paroxysmal atrial fibrillation: A systematic review and meta-analysis of randomized controlled trials. Indian Heart Journal January 2021; 73(1):63–73. ISSN 0019-4832.

[3] Aksu T, Guler TE, Bozyel S, Yalin K. Usage of a new mapping algorithm to detect possible critical substrate for continuity of atrial fibrillation: fractionation mapping in preliminary experience. J Interv Card Electrophysiol June 2020; 58(1):29–34.

[4] Campos FO, Wiener T, Prassl AJ, dos Santos RW, Sanchez-Quintana D, Ahammer H, Plank G, Hofer E. Electroanatomical characterization of atrial microfibrosis in a histologically detailed computer model. IEEE Trans Biomed Eng August 2013;60(8):2339–2349.

[5] Pachon M JC, Pachon M EI, Pachon M JC, Lobo TJ, Pachon MZ, Vargas RNA, Pachon DQV, Lopez M FJ, Jatene AD. A new treatment for atrial fibrillation based on spectral analysis to guide the catheter RF-ablation. Europace November 2004; 6(6):590–601.

[6] Halidou A, Mohamadou Y, Ari AAA, Zacko EJG. Review of wavelet denoising algorithms. Multimed Tools Appl November 2023;82(27):41539–41569.

[7] Williams SE, Roney CH, Connolly A, Sim I, Whitaker J, O’Hare D, Kotadia I, O’Neill L, Corrado C, Bishop M, Niederer SA, Wright M, O’Neill M, Linton NWF. OpenEP: A cross-platform electroanatomic mapping data format and analysis platform for electrophysiology research. Front Physiol February 2021;12:646023.

[8] Williams S, Linton N. openep/openep-core: v1.0.03, 2021.

[9] Zei P, Aguilar M, Yarnitsky J, Botzer L, Rubinstein V, Nakar E, Markides V, Derval N, Anselmino M, Winterfield J, Melby D, Marai I, Suleiman M, Meyer C. The advanced reference annotation algorithm: A novel approach to reference annotation for electroanatomic mapping. Int J Hear Rhythm 2019; 4(2):48.

Address for correspondence:

Niklas Tanger
Cardiovascular Imaging and Dynamics UZ Herestraat 49 - box 7003 3000 Leuven.
Niklas.tanger@kuleuven.be